Polymer 201 (2020) 122552

Contents lists available at ScienceDirect

Polymer

journal homepage: http://www.elsevier.com/locate/polymer

A tetraphenylethylene-functionalized benzoxazine and copper(II) acetylacetonate form a high-performance polybenzoxazine

Xian Zhang [a], Mohamed Gamal Mohamed [b,c], Zhong Xin [a,**], Shiao-Wei Kuo [b,d,*]

[a] Shanghai Key Laboratory of Multiphase Materials Chemical Engineering, Department of Product Engineering, East China University of Science and Technology, Shanghai, 200237, PR China
[b] Department of Materials and Optoelectronic Science, Center of Crystal Research, National Sun Yat-Sen University, Kaohsiung, Taiwan
[c] Chemistry Department, Faculty of Science, Assiut University, Assiut, 71516, Egypt
[d] Department of Medicinal and Applied Chemistry, Kaohsiung Medical University, Kaohsiung, 807, Taiwan

ARTICLE INFO

Keywords:
Benzoxazine
Ring-opening polymerization
Low surface free energy

ABSTRACT

In this study, we synthesized TPE-BZ, a new tetraphenylethylene (TPE)-functionalized benzoxazine (BZ) monomer (1,1,2,2-tetrakis(3-phenyl-3,4-dihydro-2H-benzo[e] [1,3]oxazin-6-yl)ethane), through reduction of the Schiff base formed from TPE-4OH–CHO (1,1,2,2-tetra(3-formyl-4-hydroxyphenyl)ethylene) and aniline and subsequent reaction with paraformaldehyde. Fourier transform infrared (FTIR) spectroscopy, nuclear magnetic resonance spectroscopy, and mass spectrometry confirmed the structure of the TPE-BZ monomer. We used differential scanning calorimetry (DSC), FTIR spectroscopy, and thermogravimetric analysis (TGA) to investigate the thermal ring opening polymerization (ROP) and thermal stability of the TPE-BZ monomer after thermal treatment at various temperatures (from room temperature to 250 °C). The TGA profiles revealed that thermal treatment at 250 °C under a N_2 atmosphere gave a poly(TPE-BZ) that possessed excellent thermal stability and a high char yield (435 °C, 64.3 wt%). Furthermore, water contact angle measurements of the poly(TPE-BZ) obtained at 210 °C for 2 h indicated a relatively low surface free energy (18.6 mJ m^{-2}), presumably because of strong intramolecular hydrogen bonding between the phenolic OH groups and the N-Mannich bridge in the polybenzoxazine matrix. We also employed DSC, FTIR spectroscopy, and TGA to examine the specific interactions in TPE-BZ/$Cu(acac)_2$ complexes. DSC analysis revealed that blending the TPE-BZ monomer with various weight ratios of $Cu(acac)_2$ lowered the thermal curing temperature of TPE-BZ from 250 to 239 °C, accompanied by a lower curing temperature at 189 °C. Using the Kissinger method, the activation energy of the TPE-BZ/$Cu(acac)_2$ complex (127 kJ mol^{-1}) was lower than that of the TPE-BZ monomer (141 kJ mol^{-1}), suggesting that $Cu(acac)_2$ functioned as a catalyst that initiated ROP of the oxazine units, while providing a product that retained high thermal stability.

1. Introduction

Polybenzoxazines (PBZs) are thermosetting resins that have attracted much attention from both industrial and academic fields because of their unique properties when compared with traditional thermosetting resins—for example, low water absorption, excellent electrical properties, high flexibility in molecular design, high thermal stability, and low surface energy (indeed, lower than that of polytetrafluoroethylene) [1,2]. PBZs have been employed in many applications, including corrosion protection, nanoimprint technology, superhydrophobic materials, and nanocomposites [3–6]. Benzoxazine (BZ) monomers are usually prepared through one-pot Mannich condensation of (para)formaldehyde, a phenol and an aromatic or primary amine [7–14]. Much literature describes methods for modifying the properties of PBZs and the development of new monomers for further application. The polymerization of BZ monomers is a thermal cationic ring-opening polymerization (ROP) of their oxazine rings, with the exothermic peak temperature typically appearing in the range 200–270 °C [11,15–17]. It would be advantageous if the processing of PBZs could be performed at lower curing temperatures. Many attempts have been made to address this issue-for example, by designing self-catalyzing BZ monomers [13,18,19] and adding Lewis acids [2,17,20] or compounds of nucleophilic

** Corresponding author.
* Corresponding author. Department of Materials and Optoelectronic Science, Center of Crystal Research, National Sun Yat-Sen University, Kaohsiung, Taiwan.
E-mail addresses: xzh@ecust.edu.cn (Z. Xin), kuosw@faculty.nsysu.edu.tw (S.-W. Kuo).

https://doi.org/10.1016/j.polymer.2020.122552
Received 17 March 2020; Received in revised form 27 April 2020; Accepted 2 May 2020
Available online 25 May 2020

character [15,21,22] to accelerate the ROP of the BZ moiety. Sudo el al [23]. reported that acetylacetonate complexes can act as catalysts for the ROP of BZ. Furthermore, many metal ions (e.g., Ti^{4+}, Al^{3+}, Fe^{3+}, Zn^{2+}, Li^{+}) can function as the effective promoters of the ROP of BZ monomers [15,17,24–26]. Hui et al. prepared a linear fluorescent tetraphenylethylene (TPE)-functionalized BZ macromolecule (TPE-BOZ) that exhibited aggregation-induced emission enhancement (AIEE) and could be used as a solid-state sensor for picric acid [27]. Recently, Xie et al. incorporated TPE into a PBZ matrix through post-modification of a main chain BZ precursor through isocyanate chemistry under simple reaction conditions; they found that a tetraphenylethene functionalized polybenzoxazines with metal complex functioned as an efficient heterogeneous catalyst for the click reaction [28]. In this present paper, we report the synthesis, thermal curing polymerization behavior, surface properties, and thermal stability of a tetrafunctional BZ monomer containing a TPE core, and its properties after blending with copper(II) acetylacetonate. We synthesized our TPE-functionalized BZ monomer, through the formation of a Schiff base from a TPE-tetracarbonyl derivative and aniline, its reduction, and subsequent oxazine ring-formation with paraformaldehyde. We used differential scanning calorimetry (DSC), temperature-dependent Fourier transform infrared (FTIR) spectroscopy, and thermogravimetric analysis (TGA) to evaluate the thermal curing polymerization behavior and thermal stability of TPE-BZ. In addition, we performed contact angle (CA) measurements to examine the surface properties of the TPE-BZ monomer before and after thermal curing at various temperatures. Finally, we employed DSC, FTIR spectroscopy, and TGA to investigate the influence of copper(II) acetylacetonate on the thermal curing polymerization behavior of the TBE-BZ monomer.

2. Experimental section

2.1. Materials

4,4′-Dihydroxybenzophenone, dimethylacetamide (DMAc), absolute EtOH (99.99%), MeOH, anhydrous magnesium sulfate ($MgSO_4$), ethyl acetate (EtOAc), tetrahydrofuran (THF), aniline, copper(II) acetylacetonate [$Cu(acac)_2$], zinc powder, titanium tetrachloride ($TiCl_4$), potassium carbonate (K_2CO_3), hexamethylenetetramine, trifluoroacetic acid (TFA), sodium borohydride ($NaBH_4$), and sodium bicarbonate ($NaHCO_3$) were purchased from Sigma–Aldrich. 1,4-Dioxane, paraformaldehyde [$(CH_2O)_n$], and acetone were purchased from Acros.

2.2. Tetra(p-hydroxyphenyl)ethylene (TPE-4OH) [29]

Zinc (2.73 g, 42.0 mmol) and anhydrous THF (80 mL) were placed in a 250-mL two-neck flask and cooled to below −10 °C under a N_2 atmosphere. $TiCl_4$ (2.34 mL, 21.5 mmol) was added slowly and then the mixture was stirred for 30 min at −10 °C before heating at 70 °C for 3 h with stirring, under a N_2 atmosphere. A solution of 4,4′-dihydroxybenzophenone (3.00 g, 14.0 mmol) in dry THF (30 mL) was added dropwise and then the mixture was heated under reflux for 24 h. Aqueous K_2CO_3 (10 wt %, 50 mL) was poured into the mixture to quench the reaction. The organic phase was separated, and the aqueous phase extracted with EtOAc (3 × 30 mL). The combined organic phases were concentrated to afford an oily residue. Recrystallization (acetone/H_2O) afforded a white powder (2.10 g, 76%). FTIR (KBr, cm^{-1}): 3650–3200 (O–H stretching) and 1611 (C═C stretching). ^{1}H NMR (DMSO-d_6, 25 °C, 500 MHz): δ (ppm) 6.48 (d, J = 8.4 Hz, 8H), 6.70 (d, J = 8.4 Hz, 8H), 9.22 (s, 4H, OH). ^{13}C NMR (DMSO-d_6, 25 °C, 500 MHz): δ (ppm) 115.12, 132.73, 135.84, 138.45, 156.26.

2.3. 1,1,2,2-Tetra(3-formyl-4-hydroxyphenyl)ethylene (TPE-4OH–CHO) [30]

A solution of TPE-4OH (1.60 g, 4.03 mmol) and hexamethylenetetramine (2.26 g, 16.1 mmol) in TFA (56.5 mL, 738.6 mmol) was heated overnight at 90 °C. Cold water was added to the mixture to afford a yellow powder (1.30 g, 82%). FTIR (KBr, cm^{-1}): 2859, 2740 (C–H stretching of CHO group), 1650 (C═O stretching). ^{1}H NMR (DMSO-d_6, 25 °C, 500 MHz): δ (ppm) 10.74 (OH), 10.11 (CHO), 7.23–6.77 (ArH). ^{13}C NMR (DMSO-d_6, 25 °C, 125 MHz): δ (ppm) 192.00, 160.47, 139.62, 138.57, 134.75, 131.60, 122.66, 117.76.

2.4. 4,4′,4′′,4′′′-(Ethene-1,1,2,2-tetrayl)tetrakis(2-((E)-(phenylimino) methyl)phenol) (TPE-aniline schiff base)

A suspension of TPE-4OH–CHO (1.21 g, 2.38 mmol) and aniline (0.97 mL, 10.74 mmol) in absolute EtOH (50 mL) was heated under reflux in a 150-mL two-neck flask for 24 h at 75 °C. The yellow solid was filtered off (1.12 g, 93%). FTIR (KBr, cm^{-1}): 3057 and 3011 (aromatic C–H stretching), 1602 (C═N stretching). ^{1}H NMR (DMSO-d_6, 25 °C, 500 MHz): δ (ppm) 10.10 (s, OH), 8.8 (s, N═C–H), 7.44–6.54 (ArH). ^{13}C NMR (DMSO-d_6, 25 °C, 125 MHz): δ (ppm) 164.01, 160.00, 149.38, 148.58, 138.54, 136.88, 135.01, 134.82, 130.20, 129.52, 127.66, 122.05, 119.68, 117.05, 116.31, 114.53. High-resolution Fourier transform mass spectrometry (HR-FTMS): calcd. for $C_{54}H_{40}N_4O_4$, m/z 809.31; found 808.30 (Fig. S1).

2.5. 4,4′,4′′,4′′′-(Ethene-1,1,2,2-tetrayl)tetrakis(2-((phenylamino) methyl)phenol) (TPE-hydroxybenzylamine)

TPE-aniline Schiff base (1.12 g, 1.58 mmol) was dissolved in DMAc (5 mL) in a 50-mL two-neck flask. After cooling at 0 °C for 30 min, $NaBH_4$ (0.300 g, 7.93 mmol) was added. The mixture was stirred overnight at 25 °C and then poured into cold water to give a brown powder (1.10 g, 98%). FTIR (KBr, cm^{-1}): 3412 (N–H stretching), 1262 (C–N stretching). ^{1}H NMR (DMSO-d_6, 25 °C, 500 MHz): δ (ppm) 9.34 (OH), 9.06 (NH), 7.06–5.35 (ArH), 4.32 (NCH_2). ^{13}C NMR (DMSO-d_6, 25 °C, 125 MHz): δ (ppm) 154.27, 150.01, 149.37, 139.17, 136.01, 133.57, 131.30, 131.43, 129.83, 128.16, 125.51, 116.74, 115.17, 113.04, 42.77. HR-FTMS: calcd. for $C_{54}H_{48}N_4O_4$, m/z 816.37; found 815.36 (Fig. S2).

2.6. 1,1,2,2-Tetrakis(3-phenyl-3,4-dihydro-2H-benzo[e] [1,3] oxazin-6-yl)ethane (TPE-BZ)

TPE-hydroxybenzylamine (1.00 g, 1.84 mmol) and paraformaldehyde (0.330 g, 11.0 mmol) were dissolved in 1,4-dioxane (40 mL) and absolute EtOH (20 mL) in a 100-mL two-neck flask. The solution was heated at 100 °C for 24 h under a N_2 atmosphere and then the solvents were evaporated under reduced pressure. The residue was dissolved in EtOAc (100 mL) and extracted with aqueous $NaHCO_3$ (2 wt %, 100 mL). The organic phase was evaporated under reduced pressure to afford a yellow solid (0.85 g, 85%). FTIR (KBr, cm^{-1}): 1231 (asymmetric C–O–C stretching), 1033 (symmetric C–O–C stretching), 937 (stretching vibrations of oxazine ring). ^{1}H NMR (DMSO-d_6, 25 °C, 500 MHz): δ (ppm) 7.24–6.42 (ArH), 5.38 (s, OCH_2N), 4.32 (s, NCH_2Ar). ^{13}C NMR (DMSO-d_6, 25 °C, 125 MHz): δ (ppm) 153.23, 148.41, 142.43, 138.96, 136.48, 130.33, 129.76, 121.18, 118.11, 116.16, 79.63 (OCH_2N), 48.95 (NCH_2Ar). FTMS: calcd. for $C_{58}H_{48}N_4O_4$, m/z 864.37; found 865.37 (Fig. S3).

2.7. Poly(TPE-BZ)

The TPE-BZ monomer (0.1 g) was thermally cured in a stepwise manner at various temperatures (110, 150, 180, 210, and 250 °C) for 2 h to give dark brown solids.

2.8. Poly(TPE-BZ) films for CA measurements

A solution of the TPE-BZ monomer (5 wt %) in dry THF was spin-

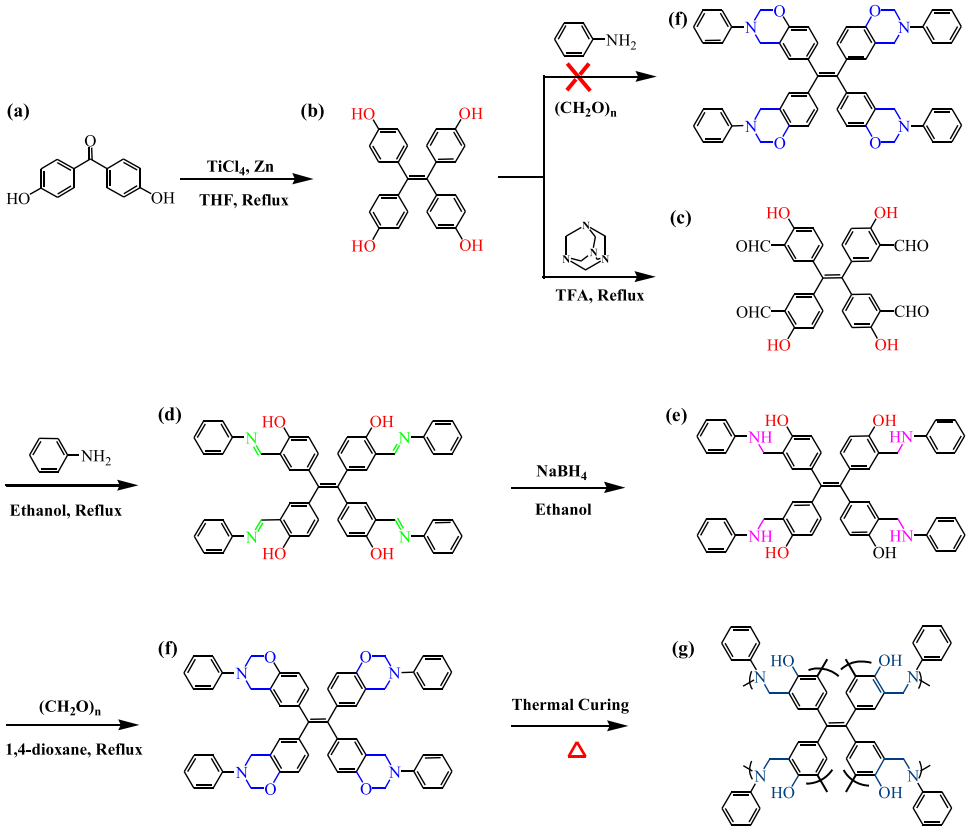

Scheme 1. Synthesis of (f) TPE-BZ from (a) 4,4′-dihydroxybenzophenone, (b) TPE-4OH, (c) TPE-4OH–CHO, (d) TPE-aniline Schiff base, and (e) TPE-hydroxybenzylamine, and the thermal curing structure of pure TPE-BZ (f) before and (g) after thermal curing.

coated (1000 rpm, 60 s) onto a substrate. The sample was cured at a temperature in the range 110–250 °C for 2 h. The surface free energies of the resulting poly(TPE-BZ) films were measured in three different solvents (deionized water, ethylene glycol, diiodomethane). The surface roughness was less than 10 nm in each case.

2.9. Poly(TPE-BZ)/Cu(acac)$_2$ complexes

Various weights ratios of Cu(acac)$_2$ and the TPE-BZ monomer were dissolved in THF (5 mL) and stirred for 24 h at room temperature. The THF from each blend sample was slowly evaporated at room temperature over 48 h. Then, each blend mixture was also thermally activated cured at 110, 150, 180, 210, and 250 °C, for 2 h at each temperature, to give their corresponding poly(TPE-BZ)/Cu(acac)$_2$ complexes.

3. Results and discussion

3.1. Synthesis of TPE-BZ monomer

Scheme 1 presents our synthesis of the TPE-BZ monomer via its *o*-hydroxybenzylamine [7,13,16,31–35]. We synthesized the *o*-hydroxybenzylamine [Scheme 1(e)] through $NaBH_4$-mediated reduction of the TPE-aniline Schiff base [Scheme 1(d)], which we obtained from the reaction of TPE-4OH–CHO with aniline in absolute EtOH [Scheme 1(c)]. Reaction of TPE-hydroxybenzylamine with paraformaldehyde gave the target TPE-functionalized BZ monomer, TPE-BZ, without any side products [Scheme 1(f)]. Unfortunately, we did not success to prepare our TPE-BZ monomer through the one-pot Mannich condensation as displayed in Scheme 1(f) which is attributed to low selectivity depending on the position of the substituents [16,31,32]. We summarized our attempt conditions [including reaction time and solvent effect] to prepare TPE-BZ through the one-pot Mannich condensation in Table S1.

The characteristic FTIR spectral absorptions of TPE-4OH [Fig. 1(a)] appear at 1611 cm^{-1} for C═C stretching and at 3650–3200 cm^{-1} for the OH groups of the phenolic units. The typical characteristics absorptions of TPE-4OH–CHO [Fig. 1(b)] are centered at 2859 and 2740 cm^{-1} for C–H stretching of the CHO groups and at 1650 cm^{-1} for C═O stretching. The absorption bands for the TPE-aniline Schiff base [Fig. 1(c)] appear at 1620 cm^{-1} for C═N stretching and at 3057 and 3011 cm^{-1} for stretching of the aromatic C–H units. After reduction of the TPE-aniline Schiff base, the signal for C═N stretching disappeared and characteristic absorptions for TPE-hydroxybenzylamine [Fig. 1(d)] appeared at 3412 cm^{-1} for N–H stretching and at 2928 cm^{-1} for stretching of the C–H aliphatic groups, indicative of complete reduction of the TPE-aniline Schiff base. The spectrum of TPE-BZ [Fig. 1(e)] features characteristic absorption bands at 1231, 1032, and 937 cm^{-1} for asymmetric and symmetric C–O–C stretching and for stretching vibrations of the oxazine ring, respectively, confirming its successful synthesis.

Fig. 2(A) displays the ^{1}H NMR spectra of TPE-4OH and TPE-4OH–CHO in DMSO-d_6. The characteristic signals of TPE-4OH [Fig. 2A(a)] were those for the OH groups of the phenolic units at 9.22 ppm and for the aromatic protons at 6.70 and 6.48 ppm. The signals of TPE-4OH–CHO [Fig. 2A(c)] nuclei. The ^{13}C NMR spectrum of TPE-4OH–CHO [Fig. 2B(d)] at 10.74, 10.11, and 7.23–6.77 ppm corresponds to the protons of the OH groups, the CHO groups, and the aromatic protons, respectively. ^{13}C NMR spectra confirmed the chemical structures of TPE-4OH and TPE-4OH–CHO. The ^{13}C NMR spectrum of TPE-4OH [Fig. 2B(b)] reveals signals at 115.12, 132.73, 135.84, 138.45, and 156.26 ppm for its aromatic carbon features signals at 192.00 ppm for its C═O carbon nuclei and 160.47, 139.62, 138.57, 134.75, 131.60, 122.66, and 117.76 ppm for its aromatic carbon nuclei.

The ^{1}H NMR spectrum of the TPE-aniline Schiff base [Fig. 3(a)]

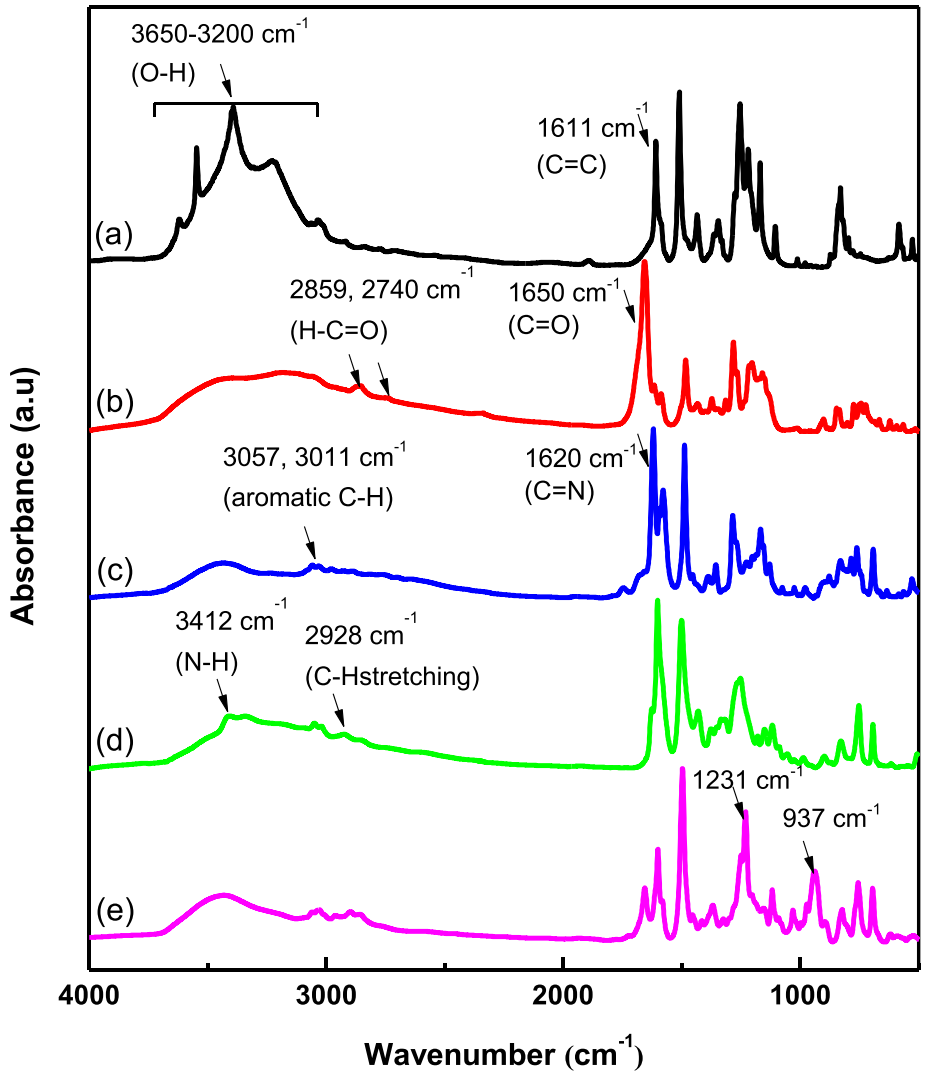

Fig. 1. FTIR spectra of (a) TPE-4OH, (b) TPE-4OH–CHO, (c) TPE-aniline Schiff base, (d) TPE-hydroxylamine, and (e) TPE-BZ, recorded at room temperature.

features signals at 10.10 and 8.88 ppm for the OH groups of the phenolic units and the N═CH groups, respectively. The ^{1}H NMR spectrum of the TPE-hydroxybenzylamine [Fig. 3(b)] features signals at 9.34 ppm for the OH groups of the phenolic units, at 9.06 ppm for the NH units, and at 7.06–5.35 ppm for the aromatic protons. The ^{1}H NMR spectrum of the TPE-BZ monomer [Fig. 3(c)] features signals at 7.24–6.42 ppm for the aromatic protons and characteristic signals for the oxazine units at 5.38 ppm (for the OCH_2N moieties) and at 4.32 ppm (for the $ArCH_2N$ moieties), confirming its successful formation.

Fig. 4 displays the ^{13}C NMR spectra of the TPE-aniline Schiff base, TPE-hydroxybenzylamine, and TPE-BZ in DMSO-d_6. The ^{13}C NMR spectrum of the TPE-aniline Schiff base [Fig. 4(a)] features signals at 164.01, 149.38, and 114.53 ppm for the COH, N═CH, and C═C carbon nuclei, respectively. The ^{13}C NMR spectrum of TPE-hydroxybenzylamine [Fig. 4(b)] features characteristic signals at 154.27–115.17, 113.04, and 42.77 ppm for its aromatic, C═C, and $NHCH_2$ carbon nuclei, respectively. In Fig. 4(c), the characteristic signals for the oxazine structures in TPE-BZ appeared at 79.63 and 48.95 ppm, for the OCH_2N and $ArCH_2N$ moieties, respectively.

We recorded FT mass spectra to confirm the synthesis of these compounds. Figs. S1, S2, and S3 reveal that the molecular weights of the TPE-aniline Schiff base, TPE-hydroxybenzylamine, and TPE-BZ monomer were *m/z* 809.31, 815.36, and 865.37, respectively, consistent with their calculated values (*m/z* 808.30, 816.37, and 864.37, respectively). Overall, the FTIR, NMR, and mass spectral data confirmed the synthesis of the TPE-BZ monomer in high purity.

3.2. Thermal polymerization of TPE-BZ

We used DSC and temperature-dependent FTIR spectroscopy to investigate the ROP behavior of the new TPE-BZ monomer. The DSC profile of TPE-BZ [Fig. 5(a)] reveals a sharp melting temperature at 114 °C, indicative of high purity, and a curing temperature of 250 °C with a reaction heat of 207 J g^{-1}. Thus, the uncured TPE-BZ monomer possessed a lower exothermic curing temperature than that of the furan containing tetrafunctional fluorene based benzoxazine monomer (t-BF-f) (279 °C) and of the cardanol containing tetrafunctional fluorene based benzoxazine monomer (t-BF-a-c) (276 °C) [35,36]. After thermal treatment of TPE-BZ at 110, 150, 180 and 210 °C, the maximum curing temperature peak appeared at 252, 250, 264, and 299 °C, respectively, with reaction heats of 201, 191, 124, and 33 J g^{-1}, respectively. Furthermore, after thermal treatment at 250 °C for 2 h, no exothermic peak was evident, indicating complete ROP of the TPE-BZ monomer and formation of poly(TPE-BZ) at this temperature. Interestingly, at 150 and 180 °C, the DSC traces of the TPE-BZ monomer exhibited glass transition temperatures at 107 and 185 °C, respectively. Fig. 5(b) presents FTIR spectra (between 2000 and 500 cm^{-1}) of TPE-BZ recorded after curing at various temperatures (from 110 to 250 °C), to reveal its polymerization

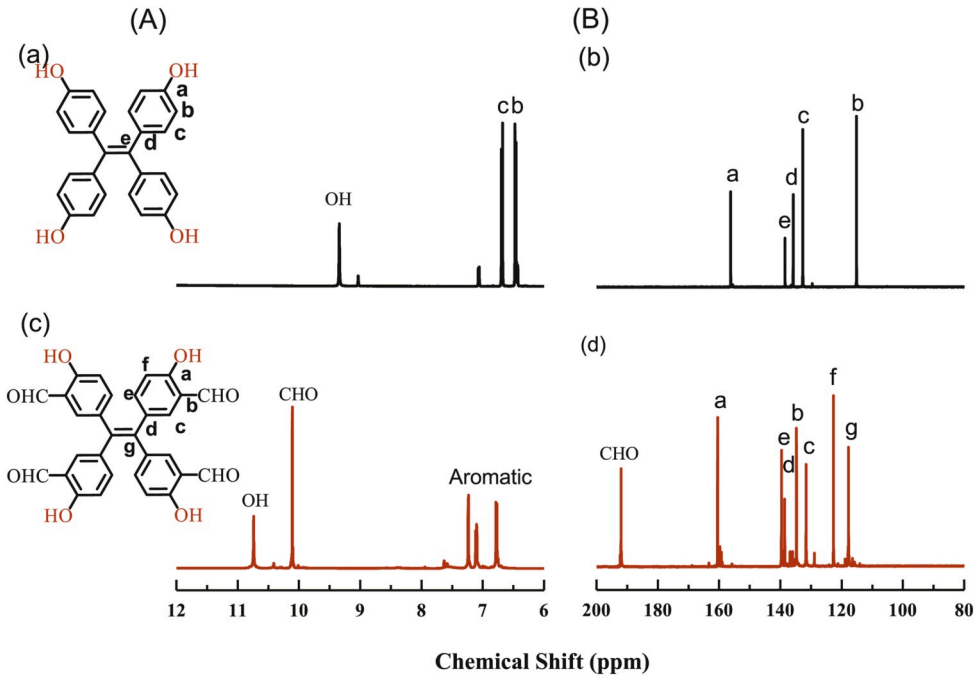

Fig. 2. (A) ^{1}H and (B) ^{13}C NMR spectra of (a, c) TPE-4OH and (b, d) TPE-4OH–CHO in DMSO-d_6.

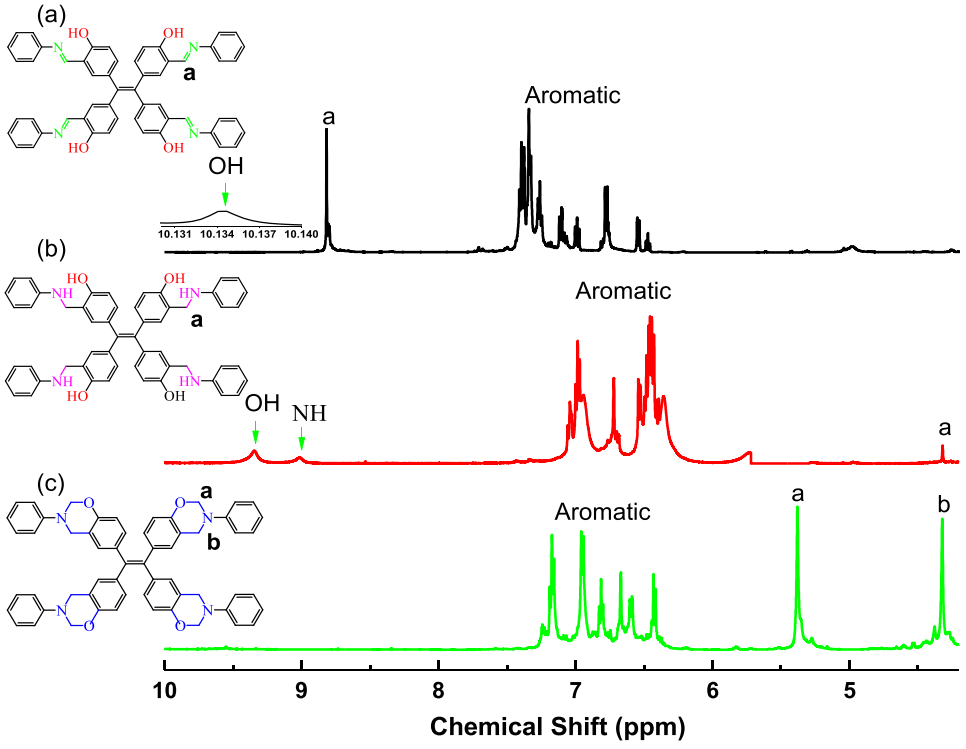

Fig. 3. ^{1}H NMR spectra of (a) TPE-aniline Schiff base, (b) TPE-hydroxylamine, and (c) TPE-BZ, recorded at room temperature.

behavior. The characteristic absorption bands of the BZ structure at 1231 (asymmetric C–O–C stretching) and 939 (BZ group) cm^{-1} disappeared almost completely after curing at 210 °C, indicative of opening of the oxazine rings. After increasing the temperature to 250 °C, the signal for the BZ ring was completely absent from the spectrum, which revealed the stable state of the polymer.

We check DMA analysis of TPE-BZ after thermal curing at 250 °C for 2 h, as displayed in Fig. S4. As shown in Fig. S4, the main T_g value of poly (TPE-BZ) was observed at 303 °C, which is smaller than that poly(t-BF-f) (440 °C) [35]. Based on TGA analysis [Fig. 6], the thermal stability and the char yield of the poly(TPE-BZ) were enhanced upon increasing the curing temperature, presumably because of a higher crosslinking density after ROP of the TPE-BZ monomer. In addition, the initial degradation temperature (T_{d10}) and the char yield increased significantly to 436 °C

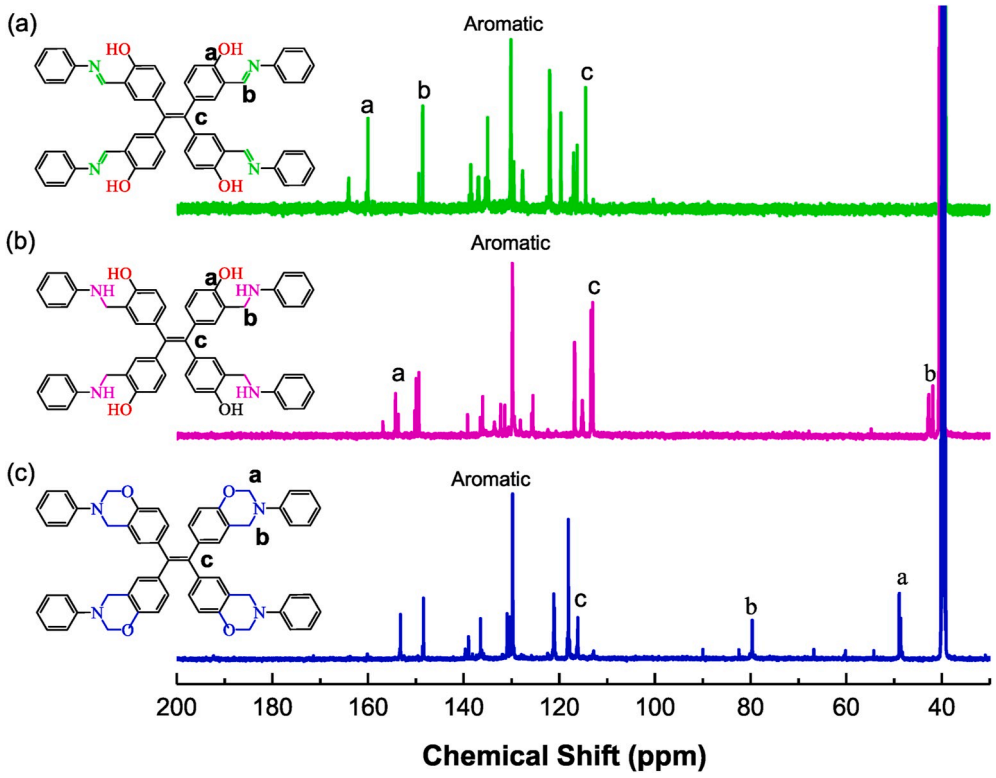

Fig. 4. ^{13}C NMR spectra of (a) TPE-aniline Schiff base, (b) TPE-hydroxylamine, and (c) TPE-BZ, recorded at room temperature.

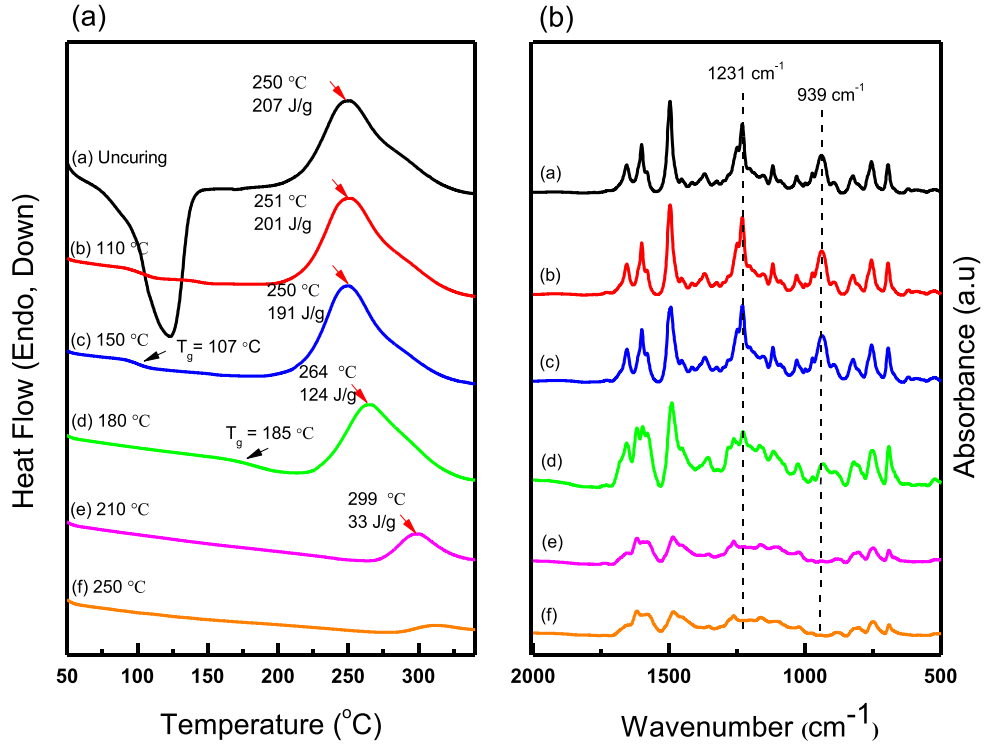

Fig. 5. (a) DSC and (b) FTIR spectral analyses of TPE-BZ after curing at various temperatures.

and 64.32 wt%, respectively, after thermal treatment at 250 °C. Our new poly(TPE-BZ) exhibited a value of T_{d10} and a char yield that are higher than that of the cardanol containing tetrafunctional fluorene based benzoxazine monomer (405 °C, 35 wt%) presumably because of the higher aromatic content in the poly(TPE-BZ) [36–40]. Table S2 summarizes the degradation temperatures and char yields of TPE-BZ before and after thermal curing at various temperature.

We performed CA measurements to examine the surface properties of the poly(TPE-BZ). The surface energy of a PBZ is related to the availability of its coordination sites and its degree of hydrogen bonding. We

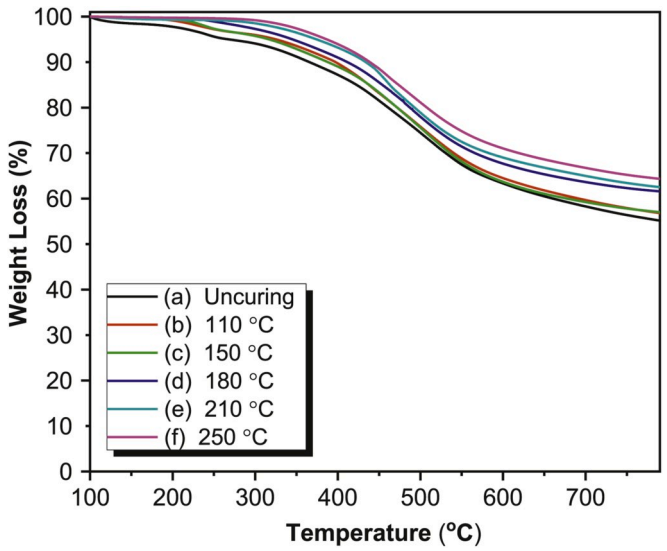

Fig. 6. TGA profiles of TPE-BZ after curing at various temperature.

Table 1
CAs (water, ethylene glycol, diiodomethane) and surface free energies of the poly(TPE-BZ) films.

Curing temperature	Contact angle (deg)			Surface free energy (mJ/m^2)
	water	ethylene glycol	diiodomethane	
RT	98.8	67.7	25.3	42.5
110 °C	100.6	72.7	37.9	37.2
150 °C	101.8	76.8	53.3	30.0
180 °C	102.2	84.9	60.8	24.8
210 °C	103.9	89.9	74.5	18.6
250 °C	92.1	78.8	69.9	23.0

examined the surface free energies (γ_s) of our poly(TPE-BZ) films that had been obtained after curing at various temperatures (from 110 to 250 °C) for 2 h, determined using three different solvents (deionized water, ethylene glycol, and diiodomethane). Fig. S5 reveals that the CAs of water were 98.8, 100.6, 101.8, 102.2, 103.9, and 92.1° before and after curing at 110, 150, 180, 210, and 250 °C, respectively; the CAs of ethylene glycol (Fig. S6) were 67.7, 72.7, 76.8, 84.9, 89.9, and 78.8°, respectively, while those of diiodomethane (Fig. S7) were 25.3, 37.9, 53.3, 60.8, 74.5, and 69.9°, respectively. We used Owens's three-liquid method to evaluate the surface free energies of these poly(TPE-BZ) films [41,42]. Table 1 reveals that the surface free energy of the poly(TPE-BZ) obtained after thermal curing at 210 °C (18.6 mJ m^{-2}) was lower than that of pure Teflon (21.0 mJ m^{-2}), due to the presence of strong intramolecular hydrogen bonding (OH···N and OH···π) after its thermal curing, as displayed in Scheme 2. Also, The value of surface free energy of the poly(TPE-BZ) increased when the curing temperature was raised to 250 °C due to increased degrees of intermolecular hydrogen bonding [43].

Previous studies have revealed that the degree of intramolecular hydrogen bonding greatly influences the surface energy of a polymeric material [6,8,35,42,43]. Our DSC thermograms [Fig. 5(a)] and FTIR spectra [Fig. 5(b)] suggested that the degree of thermal curing of poly (TPE-BZ) affected its surface free energy significantly. As reported previously, a conversion from intermolecular to intramolecular hydrogen bonding occurs during the process of curing in PBZ systems, and there exists a critical degree of curing that provides the lowest surface free energy.[8] Our surface free energy data are in a good agreement with those of previous studies [8,35,42,44].

3.3. Thermal polymerization of TPE-BZ/Cu(acac)$_2$ complexes

We used DSC to study the thermal curing behavior of the TPE-BZ monomer in the presence of various amounts of Cu(acac)$_2$ under N_2 at heating rate 20 °C min^{-1} (Fig. 7). The endothermic peak that represented from melting of TPE-BZ disappeared after blending with Cu(acac)$_2$, indicating that the crystallinity of TPE-BZ was destroyed upon its interaction with Cu(acac)$_2$ [45]. The addition of Cu(acac)$_2$ altered the polymerization behavior of TPE-BZ drastically, occurring at a very low temperature and resulting in two exotherms. The first curing peak appeared at 189.4 °C, presumably related to ring opening of the BZ units coordinated with Cu^{2+} ions; the second curing peak represented curing of the non-coordinated BZ units [16,44]. After the addition 10 wt % of Cu(acac)$_2$, the curing temperature of TPE-BZ shifted from 250.6 to 239.5 °C, accompanied by an increase in the intensity of peak for the lower curing temperature at 189.4 °C. From these data, we conclude that

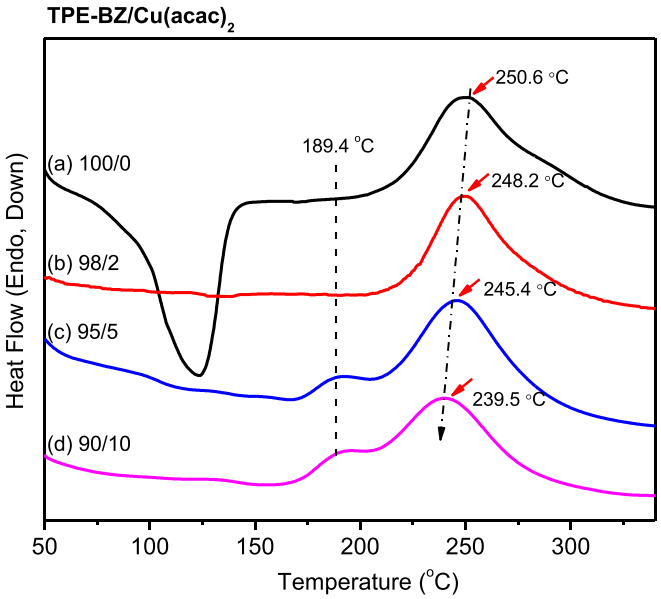

Fig. 7. DSC thermograms of TPE-BZ/Cu(acac)$_2$ complexes prepared at weight ratios of (a) 100/0, (b) 98/2, (c) 95/5, and (d) 90/10.

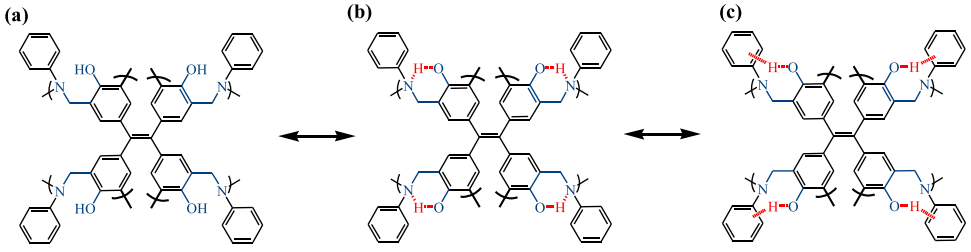

Scheme 2. The intramolecular hydrogen bonding in poly(TPE-BZ).

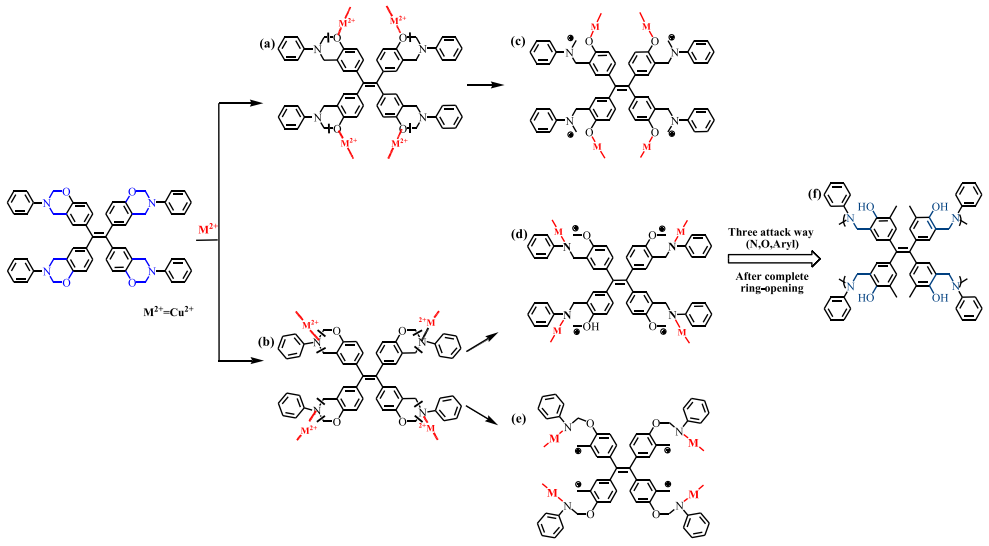

Scheme 3. The mechanism of the ring-opening polymerization of TPE-BZ with Cu^{2+} ions.

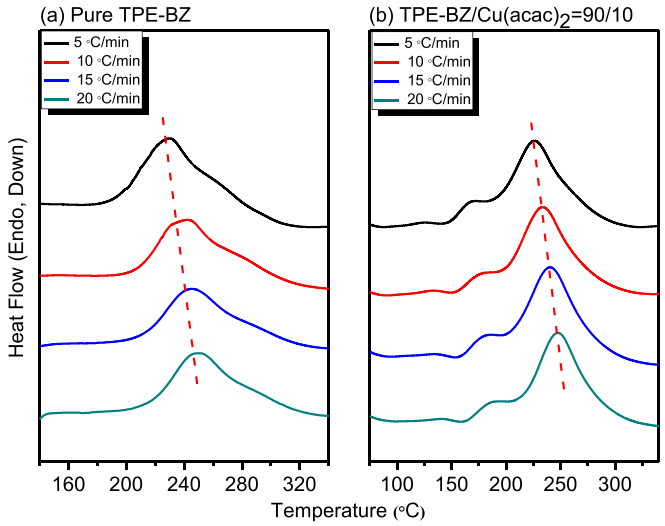

Fig. 8. Dynamic DSC exothermic curves of (a) pure TPE-BZ and (b) the TPE-BZ/$Cu(acac)_2$ = 90/10 complex, recorded at various heating rates.

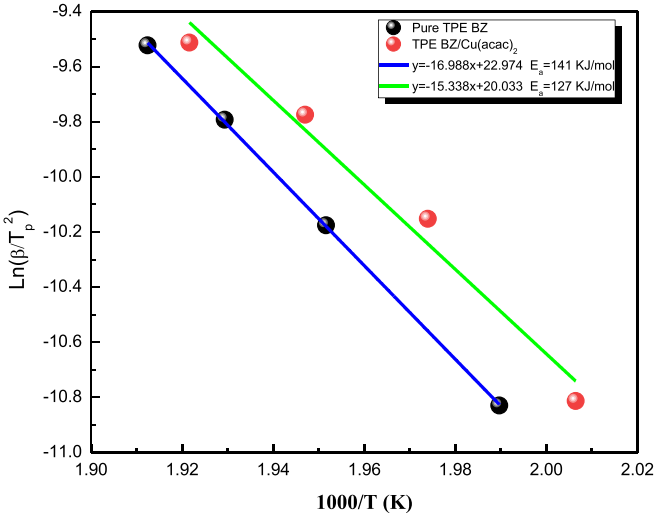

Fig. 9. Kissinger plots (for determination of values of Ea) of the pure TPE-BZ and the TPE-BZ/$Cu(acac)_2$ = 90/10 complex.

$Cu(acac)_2$ can promote the ring opening of oxazine rings at a lower temperature and that the Cu^{2+} ions acted as catalysts that initiated the ring-opening process [46]. Scheme 3 presents the mechanism for the coordination of Cu^{2+} ions to TPE-BZ and for the ROP of the oxazine units [17,39].

Initially, the Cu^{2+} ions coordinate with oxygen or nitrogen atoms in the oxazine ring; next, electrophilic attack of the Cu^{2+} ions to the oxazine ring occurs through O-, N-, and aryl-attack; finally, rearrangement occurs to form a stable structure [2,17]. Because $Cu(acac)_2$ could act as a catalyst and enhance the ROP of the oxazine units in TPE-BZ, we used non-isothermal DSC at various heating rates to study the influence of $Cu(acac)_2$ on the polymerization kinetics of TPE-BZ (Fig. 8). We applied the Kissinger method to investigate the curing kinetics of our BZ system [47]. Based on this method, we calculated the activation energies of TPE-BZ and TPE-BZ/$Cu(acac)_2$ according to equation (1):

$$In\left(\frac{\beta}{T_p^2}\right) = In\left(\frac{AR}{E_a}\right) - \frac{E_a}{RT} \quad (1)$$

where β (equal to dT/dt) is the heating rate, A is the pre-exponential factor, T_P is the exothermic curing peak, and R is the universal gas constant. Fig. 8 presents the plot of $\ln(\beta/T_P^2)$ with respect to $1/T_P^2$, which, according to the Kissinger method, provides the value of E_a from the slope of the line.

The calculated activation energies were 141 kJ mol^{-1} for the pure TPE-BZ and 127 kJ mol^{-1} for the TPE-BZ/$Cu(acac)_2$ complex. These values suggest that TPE-BZ/$Cu(acac)_2$ is activated for polymerization; in other words, $Cu(acac)_2$ can act as a catalyst to enhance the ROP of the oxazine units [48–51]. Notably, the activation energy for the polymerization of TPE-BZ is higher than those for other BZ resins, suggesting that TPE-BZ monomer is not readily polymerized to give poly(TPE-BZ) because of its highly rigid structure. To examine the degree of thermal cross-linking after the addition of $Cu(acac)_2$ into the TPE-BZ system, we used DSC and FTIR spectroscopy to evaluate the thermal ROP of TPE-BZ in the presence of 10 wt % $Cu(acac)_2$ (Fig. 9).

We recorded the DSC thermograms of TPE-BZ/$Cu(acac)_2$ after curing for 2 h at temperatures of 110, 150, 180, 210, and 250 °C, respectively. Fig. 10(a) reveals that the two thermal curing peaks of the non-cured TPE-BZ/$Cu(acac)_2$ = 90/10 complex were centered at 183 and 241 °C, respectively. The maximum exothermic peak of TPE-BZ/$Cu(acac)_2$

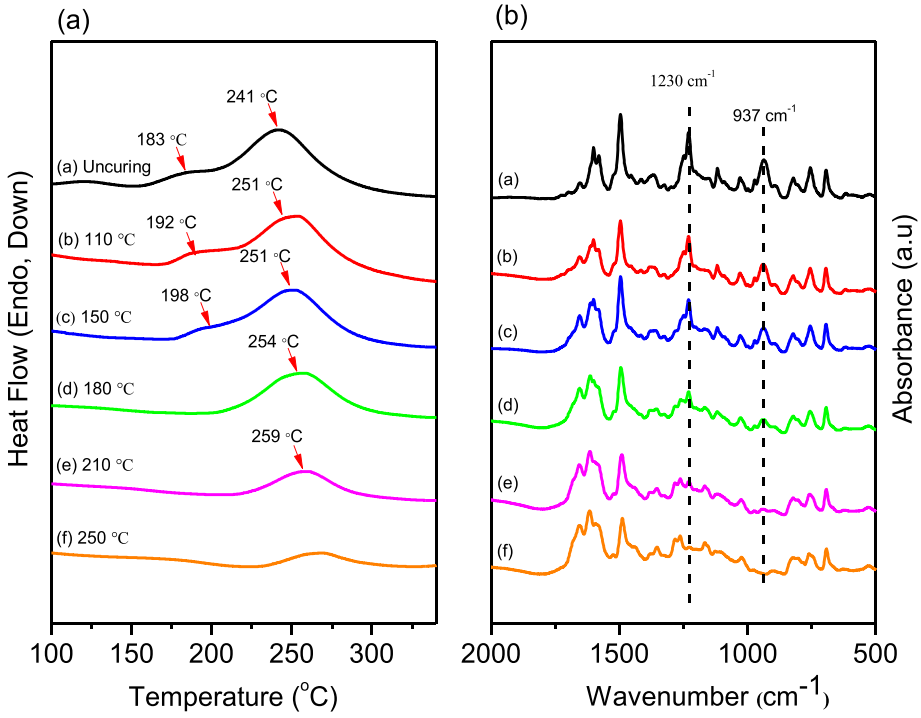

Fig. 10. (a) DSC and (b) FTIR spectral analyses of the TPE-BZ/Cu(acac)$_2$ = 90/10 complex at various temperatures.

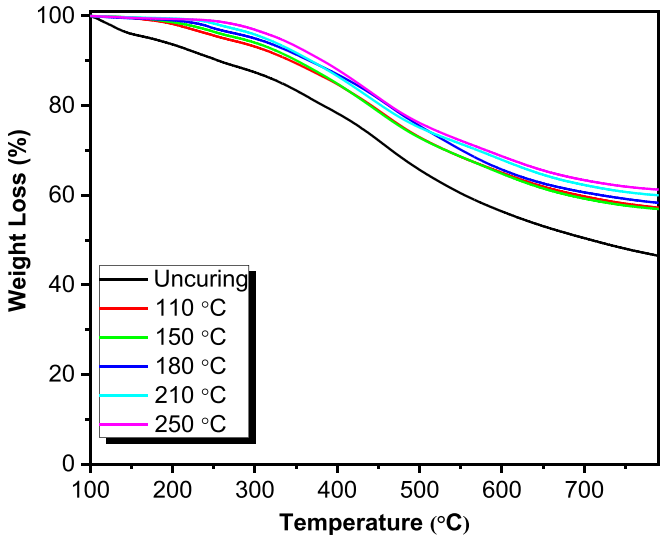

Fig. 11. TGA profiles of TPE-BZ/Cu(acac)$_2$ complexes after thermal treatment at various temperatures.

decreased gradually, and eventually disappeared completely, upon increasing the curing temperature from 110 to 250 °C. Although this behavior is consistent with the thermal curing behavior of the pure TPE-BZ, under the same thermal conditions the exothermic peak of TPE-BZ/Cu(acac)$_2$ was much lower than that of the pure monomer. For example, the curing temperature peak appeared at 259 °C for TPE-BZ/Cu(acac)$_2$ and at 299 °C for the pure TPE-BZ after thermal curing at 210 °C for 2 h, indicating that the ring-opening process of TPE-BZ/Cu(acac)$_2$ was much more facile than that of the pure monomer. We also used FTIR spectroscopy to investigate the thermal curing polymerization behavior of the TPE-BZ/Cu(acac)$_2$ = 90/10 complex at various curing temperatures. The absorption signals representing the BZ rings [at 1230 (asymmetric C–O–C stretching) and 934 (benzene with an attached oxazine ring) cm^{-1}] gradually disappeared upon increasing the curing temperature from 110 to 250 °C [Fig. 10(b)].

This phenomenon arose from a combination of ring-opening of the BZ monomer and the formation of poly(TPE-BZ)/Cu(acac)$_2$. The FTIR spectral data are consistent with the results of the DSC analyses, and confirmed that the thermal ROP was initiated at lower curing temperatures and was complete at higher curing temperatures. Fig. 11 displays the thermal stability of the TPE-BZ/Cu(acac)$_2$ = 90/10 complex before and after thermal curing at 110, 150, 180, 210, and 250 °C under N_2 at heating rate 20 °C min^{-1}. The value of T_{d5} and the char yield of poly(TPE-BZ)/Cu(acac)$_2$ systems all increased upon increasing the curing temperature, consistent with an increase in the crosslinking density after ROP. Thus, the addition of Cu(acac)$_2$ facilitated ring opening of the TPE-BZ monomer, but it did not decrease the thermal stability or the char yield significantly, based on TGA analyses.

4. Conclusions

We have synthesized TPE-BZ, a new TPE-functionalized BZ monomer, through reduction of a TPE-aniline Schiff base and subsequent oxazine ring formation with paraformaldehyde. FTIR, NMR, and FTMS spectra confirmed the chemical structures and purity of all the synthesized compounds. The resultant poly(TPE-BZ) exhibited excellent thermal stability and high char yields after thermal treatment, due to increases in their crosslinking density. The poly(TPE-BZ) had relatively low surface free energies; the lowest value was 18.6 mJ m^{-2}, for the sample obtained after curing at 210 °C for 2 h. In addition, the curing temperature of the TPE-BZ/Cu(acac)$_2$ complex [containing 10 wt % Cu(acac)$_2$)] shifted from 250.6 to 239.5 °C, accompanied by a lower curing temperature centered at 189.4 °C. In addition, the calculated activation energy of the TPE-BZ/Cu(acac)$_2$ system was lower than that of the pure TPE-BZ monomer, indicating that Cu(acac)$_2$ acted as a catalyst that initiated ROP of the oxazine units.

Declaration of competing interest

There are no conflicts to declare.

CRediT authorship contribution statement

Xian Zhang: Conceptualization, Data curation, Formal analysis. **Mohamed Gamal Mohamed:** Conceptualization, Data curation, Formal analysis, Investigation, Methodology, Writing - original draft. **Zhong Xin:** Supervision, Writing - original draft, Writing - review & editing. **Shiao-Wei Kuo:** Supervision, Writing - original draft, Writing - review & editing.

Acknowledgements

This study was supported financially by the Ministry of Science and Technology, Taiwan, under contracts MOST 106-2221-E-110- 067-MY3, 108-2638-E-002-003-MY2, and 108-2221-E-110-014-MY3.

Appendix A. Supplementary data

Supplementary data to this article can be found online at https://doi.org/10.1016/j.polymer.2020.122552.

References

[1] K. Zhang, Q. Zhuang, X. Liu, G. Yang, R. Cai, Z. Han, A new benzoxazine containing benzoxazole-functionalized polyhedral oligomeric silsesquioxane and the corresponding polybenzoxazine nanocomposites, Macromolecules 46 (2013) 2696–2704.
[2] S. Zhang, Q. Ran, Q. Fu, Y. Gu, Thermal responsiveness of hydrogen bonding and dielectric property of polybenzoxazines with different Mannich bridge structures, Polymer 175 (2019) 302–309.
[3] X. Liu, R. Zhang, T. Li, P. Zhu, Q. Zhuang, Novel fully biobased benzoxazines from rosin: synthesis and properties, ACS Sustain. Chem. Eng. 5 (2017) 10682–10692.
[4] L. Qu, Z. Xin, Preparation and surface properties of novel low surface free energy fluorinated silane-functional polybenzoxazine films, Langmuir 27 (2011) 8365–8370.
[5] M.G. Mohamed, S.W. Kuo, Functional silica and carbon nanocomposites based on polybenzoxazines, Macromol. Chem. Phys. 220 (2019) 1800306.
[6] W.C. Chen, S.W. Kuo, Ortho-Imide and allyl groups effect on highly thermally stable polybenzoxazine/double-decker-shaped polyhedral silsesquioxane hybrids, Macromolecules 51 (2018) 9602–9612.
[7] X. Liu, Z. Li, G. Zhan, Y. Wu, Q. Zhuang, Bio-based benzoxazines based on sesamol: synthesis and properties, J. Appl. Polym. Sci. 136 (2019) 48255–48262.
[8] J. Liu, X. Lu, Z. Xin, C. Zhou, Synthesis, and surface properties of low surface free energy silane-functional polybenzoxazine films, Langmuir 29 (2012) 411–416.
[9] R.C. Lin, M.G. Mohamed, K.C. Hsu, J.Y. Wu, Y.R. Jheng, S.W. Kuo, Multivalent photo-crosslinkable coumarin-containing polybenzoxazines exhibiting enhanced thermal and hydrophobic surface properties, RSC Adv. 6 (2016) 10683–10696.
[10] H.R. Abuzeid, M.M.M. Ahmed, A.F.M. EL-Mahdy, S.W. Kuo, Triazine-functionalized covalent benzoxazine framework for directly synthesis of N-doped microporous carbon, Polym. Chem. 10 (2019) 6010–6020.
[11] S. Shukla, A. Mahata, B. Pathak, B. Lochab, Cardanol benzoxazines–interplay of oxazine functionality (mono to tetra) and properties, RSC Adv. 5 (2015) 78071–78080.
[12] M.G. Mohamed, K.C. Hsu, S.W. Kuo, Bifunctional polybenzoxazine nanocomposites containing photo-crosslinkable coumarin units and pyrene units capable of dispersing single-walled carbon nanotubes, Polym. Chem. 6 (2015) 2423–2433.
[13] W. Zhang, P. Froimowicz, C.R. Arza, S. Ohashi, H. Ishida, Latent catalyst-containing naphthoxazine: synthesis and effects on ring-opening polymerization, Macromolecules 49 (2016) 7129–7140.
[14] K. Zhang, X. Yu, S.W. Kuo, Outstanding dielectric, and thermal properties of main chain-type poly(benzoxazine-co-imide-co-siloxane)-based cross-linked networks, Polym. Chem. 10 (2019) 2387–2396.
[15] A. Kocaarslan, B. Kiskan, Y. Yagci, Ammonium salt catalyzed ring-opening polymerization of 1, 3-benzoxazines, Polymer 122 (2017) 340–346.
[16] S. Ohashi, V. Pandey, C.R. Arza, P. Froimowicz, H. Ishida, Simple and low energy consuming synthesis of cyanate ester functional naphthoxazines and their properties, Polym. Chem. 7 (2016) 2245–2252.
[17] C. Liu, D. Shen, R.M. Sebastián, J. Marquet, R. Schönfeld, Catalyst effects on the ring-opening polymerization of 1,3-benzoxazine and on the polymer structure, Polymer 54 (2013) 2873–2878.
[18] G. Kaya, B. Kiskan, Y. Yagci, Phenolic naphthoxazines as curing promoters for benzoxazines, Macromolecules 51 (2018) 1688–1695.
[19] K. Zhang, X. Yu, Y. Wang, Y. Liu, Thermally activated structural changes of a norbornene–benzoxazine–phthalonitrile thermosetting system: simple synthesis, self-catalyzed polymerization, and outstanding flame retardancy, ACS Appl. Polym. Mater. 1 (2019) 2713–2722.
[20] S.N. Kolanadiyil, M. Azechi, T. Endo, Synthesis of novel tri-benzoxazine and effect of phenolic nucleophiles on its ring-opening polymerization, J. Polym. Sci., Part A: Polym. Chem. 54 (2016) 2811–2819.
[21] L. Zhang, J. Mao, S. Wang, Y. Yang, Y. Chen, H. Lu, Meta-phenylenediamine formaldehyde oligomer: a new accelerator for benzoxazine resin, React. Funct. Polym. 121 (2017) 51–57.
[22] J. Sun, W. Wei, Y. Xu, J. Qu, X. Liu, T. Endo, A curing system of benzoxazine with amine: reactivity, reaction mechanism and material properties, RSC Adv. 5 (2015) 19048–19057.
[23] A. Sudo, S. Hirayama, T. Endo, Highly efficient catalysts-acetylacetonato complexes of transition metals in the 4th period for ring-opening polymerization of 1, 3-benzoxazine, J. Polym. Sci., Part A: Polym. Chem. 48 (2010) 479–484.
[24] M.G. Mohamed, S.W. Kuo, Crown ether–functionalized polybenzoxazine for metal ion Adsorption, Macromolecules 53 (2020) 2420–2429.
[25] B. Kiskan, Y. Yagci, E. Sahmetlioglu, L. Toppare, Preparation of conductive polybenzoxazines by oxidative polymerization, J. Polym. Sci., Part A: Polym. Chem. 45 (2007) 999–1006.
[26] M.G. Mohamed, R.C. Lin, J.H. Tu, F.H. Lu, J.L. Hong, K.U. Jeong, C.F. Wang, S. W. Kuo, Thermal property of an aggregation-induced emission fluorophore that forms metal–ligand complexes with $Zn(ClO_4)_2$ of salicylaldehyde azine-functionalized polybenzoxazine, RSC Adv. 5 (2015) 65635–65645.
[27] Y. Su, W. Shi, X. Chen, S. Zhao, Y. Hui, Z. Xie, An aggregation-induced emission enhancement fluorescent benzoxazine-derived macromolecule: catalyst-free synthesis and its preliminary application for the determination of aqueous picric acid, RSC Adv. 6 (2016) 41340–41347.
[28] W. Shi, Q. Liu, J. Zhang, X. Zhou, C. Yang, K. Zhang, Z. Xie, Tetraphenylethene-decorated functional polybenzoxazines: post-polymerization synthesis via benzoxazine–isocyanide chemistry and application in probing and catalyst fields, Polym. Chem. 10 (2019) 1130–1139.
[29] J. Li, K. Shi, M. Drechsler, B.Z. Tang, J. Huang, Y. Yan, A supramolecular fluorescent vesicle based on a coordinating aggregation induced emission amphiphile: insight into the role of electrical charge in cancer cell division, Chem. Commun. 52 (2016) 12466–12469.
[30] J.B. Xiong, Y.X. Yuan, L. Wang, J.P. Sun, W.G. Qiao, H.C. Zhang, M. Duan, H. Han, S. Zhang, Y.S. Zheng, Evidence for aggregation-induced emission from free rotation restriction of double bond at excited state, Org. Lett. 20 (2018) 373–376.
[31] S. Ohashi, F. Cassidy, S. Huang, K. Chiou, H. Ishida, Synthesis and ring-opening polymerization of 2-substituted 1, 3-benzoxazine: the first observation of the polymerization of oxazine ring-substituted benzoxazines, Polym. Chem. 7 (2016) 7177–7184.
[32] C.H. Lin, S.L. Chang, C.W. Hsieh, H.H. Lee, Aromatic diamine-based benzoxazines and their high-performance thermosets, Polymer 49 (2008) 1220–1229.
[33] C.R. Arza, P. Froimowicz, L. Han, R. Graf, H. Ishida, Design, synthesis, characterization, and polymerization of fused ring naphthoxazine resins, Macromolecules 50 (2017) 9249–9256.
[34] N.K. Sini, T. Endo, Toward elucidating the role of number of oxazine rings and intermediates in the benzoxazine backbone on their thermal characteristics, Macromolecules 49 (2016) 8466–8478.
[35] H. Wang, J. Wang, X. He, T. Feng, N. Ramdani, M. Luan, W. Liu, X. Xu, Synthesis of novel furan-containing tetrafunctional fluorene-based benzoxazine monomer and its high-performance thermoset, RSC Adv. 4 (2014) 64798–64801.
[36] Y.P. Chen, X.Y. He, A.Q. Dayo, J.Y. Wang, W. Liu, J. Wang, T. Tang, Synthesis and characterization of cardanol containing tetra-functional fluorene-based benzoxazine resin having two different oxazine ring structures, Polymer 179 (2019) 121620–121626.
[37] H. Dong, Z. Xin, X. Lu, Y. Lv, Effect of N-substituents on the surface characteristics and hydrogen bonding network of polybenzoxazines, Polymer 52 (2011) 1092–1101.
[38] M.G. Mohamed, C.H. Hsiao, K.C. Hsu, F.H. Lu, H.K. Shih, S.W. Kuo, Supramolecular functionalized polybenzoxazines from azobenzene carboxylic acid/azobenzene pyridine complexes: synthesis, surface properties, and specific interactions, RSC Adv. 5 (2015) 12763–12772.
[39] C. Liu, D. Shen, R.M. Sebastián, J. Marquet, R. Schönfeld, Mechanistic studies on ring-opening polymerization of benzoxazines: a mechanistically based catalyst design, Macromolecules 44 (2011) 4616–4622.
[40] H.J. Kim, Z. Brunovska, H. Ishida, Synthesis and thermal characterization of polybenzoxazines based on acetylene-functional monomers, Polymer 40 (1999) 6565–6573.
[41] J. Tsibouklis, M. Stone, A.A. Thorpe, P. Graham, T.G. Nevell, R.J. Ewen, Surface energy characteristics of polymer film Structures: A further insight into the molecular design requirements, Langmuir 15 (1999) 7076–7079.
[42] D.K. Owens, R.C. Wendt, Estimation of the surface free energy of polymers, J. Appl. Polym. Sci. 13 (1969) 1741–1747.
[43] C.F. Wang, Y.C. Su, S.W. Kuo, C.F. Huang, Y.C. Sheen, F.C. Chang, Low-surface-free-energy materials based on polybenzoxazines, Angew. Chem. Int. Ed. 45 (2006) 2248–2251.
[44] H.D. Kim, H. Ishida, A study on hydrogen bonding in controlled structure benzoxazine model oligomers, Macromol. Symp. 195 (2003) 123–140.
[45] M.G. Mohamed, W.C. Su, Y.C. Lin, C.F. Wang, J.K. Chen, K.U. Jeong, S.W. Kuo, Azopyridine-functionalized benzoxazine with $Zn(ClO_4)_2$ form high-performance polybenzoxazine stabilized through metal–ligand coordination, RSC Adv. 4 (2014) 50373–50385.
[46] H.Y. Low, H. Ishida, Improved thermal stability of polybenzoxazines by transition metals, Polym. Degrad. Stabil. 91 (2006) 805–815.
[47] H.E. Kissinger, Reaction kinetics in differential thermal analysis, Anal. Chem. 29 (1957) 1702–1706.
[48] Y. Lu, M. Li, Y. Zhang, D. Hu, L. Ke, W. Xu, Synthesis and curing kinetics of benzoxazine containing fluorene and furan groups, Thermochim. Acta 515 (2011) 32–37.

[49] K. Zhang, Q.X. Zhuang, Y.C. Zhou, X.Y. Liu, G. Yang, Z.W. Han, Preparation and properties of novel low dielectric constant benzoxazole-based polybenzoxazine, J. Polym. Sci., Part A: Polym. Chem. 50 (2012) 5115–5123.
[50] H. Ishida, Y. Rodriguez, Curing kinetics of a new benzoxazine-based phenolic resin by differential scanning calorimetry, Polymer 36 (1995) 3151–3158.
[51] M.L. Salum, D. Iguchi, C.R. Arza, L. Han, H. Ishida, P. Froimowicz, Making benzoxazines greener: design, synthesis, and polymerization of a biobased benzoxazine fulfilling two principles of green chemistry, ACS Sustain. Chem. Eng. 6 (2018) 13096–13106.